nature biomedical engineering

ARTICLES
https://doi.org/10.1038/s41551-022-00918-x

Check for updates

A low-power stretchable neuromorphic nerve with proprioceptive feedback

Yeongjun Lee[1,2,8], Yuxin Liu[3,4,8], Dae-Gyo Seo[1,8], Jin Young Oh[2], Yeongin Kim[5], Jinxing Li[2], Jiheong Kang[2], Jaemin Kim[2], Jaewan Mun[2], Amir M. Foudeh[2], Zhenan Bao[2] ✉ and Tae-Woo Lee[1,6,7] ✉

By relaying neural signals from the motor cortex to muscles, devices for neurorehabilitation can enhance the movement of limbs in which nerves have been damaged as a consequence of injuries affecting the spinal cord or the lower motor neurons. However, conventional neuroprosthetic devices are rigid and power-hungry. Here we report a stretchable neuromorphic implant that restores coordinated and smooth motions in the legs of mice with neurological motor disorders, enabling the animals to kick a ball, walk or run. The neuromorphic implant acts as an artificial efferent nerve by generating electrophysiological signals from excitatory post-synaptic signals and by providing proprioceptive feedback. The device operates at low power (~1/150 that of a typical microprocessor system), and consists of hydrogel electrodes connected to a stretchable transistor incorporating an organic semiconducting nanowire (acting as an artificial synapse), connected via an ion gel to an artificial proprioceptor incorporating a carbon nanotube strain sensor (acting as an artificial muscle spindle). Stretchable electronics with proprioceptive feedback may inspire the further development of advanced neuromorphic devices for neurorehabilitation.

Neurological diseases can lead to poor quality of life and even death[1]. In particular, spinal cord injuries (SCIs) and motor neuron diseases (MNDs) prevent the transmission of neural signals from the primary motor cortex to muscles, and thereby limit the movements of the body and substantially impair the quality of life of patients with these diseases. Cellular and molecular treatments[2,3] aim at the complete recovery of damaged nerves, yet restoring motor function in them has long been a hard problem to solve. Instead, temporizing neurorehabilitation devices that aim to restore motor functions of patients can improve quality of life[4]. Neurorehabilitation devices can effectively and reliably redirect biosignals to bypass damaged neural components and restore motor functions[5,6], but conventional systems that use a von Neumann architecture consume high amounts of power and lack the neuroplasticity of their biological counterpart. Also, conventional stimulation uses electrical pulses with constant amplitude, which often induce abrupt and drastic contraction of the muscles[7], and because muscle contraction force is difficult to predict, this causes discomfort to the user[8]. To generate movements that are more natural and that ensure patient comfort, voltage ramping has been used during stimulation onset and de-activation[9,10], but this method requires additional function generators. In addition, their rigid nature causes discomfort. These limitations could be solved by using neuroprosthetic electronic nerves that exploit neuroplasticity, are highly stretchable and emulate the event-driven synaptic signal transmission in biological peripheral nerves without the use of external high-power computing units[11,12].

Artificial peripheral nerves that emulate biological afferent and efferent nerves and that deliver sensory[13–20] and motor[21–25] information with spike-driven neural plasticity are becoming important technologies for the realization of bioinspired electronic skins[26,27], intelligent robotics[28] and neurorehabilitation devices[29–31]. Artificial peripheral nerves that mimic the signal processing and functionality of biological nerves can restore impaired biosignal communication when integrated with biological systems[29–31]. An organic afferent (or sensory) nerve has been linked with an insect's leg to demonstrate simple reflex action[31], but no research has demonstrated artificial efferent (or motor) nerves that control biological motor responses in vertebrates, which is an essential ability in future biocompatible and energy-efficient neurorehabilitation devices. Practical applications of such systems for brain-directed limb movement in vertebrates, including humans, require the coordinated and voluntary control of limbs. In addition to signalling through artificial peripheral nerves, the realization of proprioception in neurorehabilitation devices is a necessary requirement to restore proper movement as well as the sense of body position. Moreover, the device must exploit the principles of neural processing that emulate biological synaptic behaviours and should operate with low energy consumption[32,33], be easily fabricated and have similar mechanical properties as soft tissues[34–36].

In this Article, we describe a stretchable neuromorphic efferent nerve (SNEN) that uses stretchable organic nanowire synaptic transistors. The SNEN can bypass a broken electrophysiological signal path (for example, those caused by SCI or MND) and redirect electrophysiological signals to control body movement with soft neural interfaces and stretchable electronic systems in a mouse model with neurological motor disorder. The synaptic signal potentiation of the neuromorphic system inherently represents electrical signal ramping, which in principle would improve natural motion and patient comfort without the use of additional bulky electronic components such as function generators. The resultant muscle force response is gradually increased, contrary to the abrupt increases

[1]Department of Materials Science and Engineering, Seoul National University, Seoul, Republic of Korea. [2]Department of Chemical Engineering, Stanford University, Stanford, CA, USA. [3]Department of Bioengineering, Stanford University, Stanford, CA, USA. [4]Department of Biomedical Engineering, National University of Singapore, Singapore, Singapore. [5]Department of Electrical Engineering, Stanford University, Stanford, CA, USA. [6]School of Chemical and Biological Engineering, Seoul National University, Seoul, Republic of Korea. [7]Institute of Engineering Research, Research Institute of Advanced Materials, Soft Foundry, Seoul National University, Seoul, Republic of Korea. [8]These authors contributed equally: Yeongjun Lee, Yuxin Liu, Dae-Gyo Seo. ✉e-mail: zbao@stanford.edu; twlees@snu.ac.kr

and decreases induced by conventional systems. The SNEN operates at ~1/150 of the power consumption of a von Neumann architecture system that uses microprocessors. Similarly to the biological motor response of animals, we controlled the displacement and maximum force of the mouse's leg via the firing rate in the artificial efferent nerve. We incorporated an artificial muscle spindle into the synaptic transistor to provide proprioceptive feedback and to prevent overstraining of the muscle. We show coordinated muscle flexion and extension, and practical motions such as walking and running, in a live animal. Furthermore, the feasibility of relaying electrophysiological signals recorded from the motor cortex of a behaving animal to control leg movement supports the further development of SNEN technology for use in future neuromorphic neurorehabilitation devices. SNEN technology might eventually allow for the generation of voluntary motion in patients with motor disorders.

Design of the SNEN

The concept of SNEN is to bypass the spinal injury or damaged nerve and send neuromorphic electrical signals to the muscles, as a functional replacement of a damaged nerve (Fig. 1a). To demonstrate this concept, the SNEN was attached to the leg or back of a mouse (Fig. 1b and Supplementary Fig. 1). The SNEN is composed of stretchable components, including a carbon nanotube (CNT) strain sensor in an artificial proprioceptor, an organic semiconducting nanowire and an ion gel in a stretchable synaptic transistor, and soft hydrogel electrodes (Fig. 1c). Biomimetic input action potential (AP) signals were applied to the artificial proprioceptor, then transferred to the synaptic transistor. CNT strain sensor (artificial muscle spindle) detected the muscle strain and regulated the output voltage of the artificial proprioceptor, which is a voltage divider. The analogue feedback-controlled pre-synaptic voltage pulses were applied to the gate electrode of artificial synaptic transistor, and resultant post-synaptic drain output signals were used to stimulate the muscles of the mouse's legs. In the artificial synaptic transistor, as the frequency of pre-synaptic gate voltage spikes (APs) was increased from 1 Hz to 11 Hz, excitatory post-synaptic current (EPSC) read by drain electrode increased (Fig. 1d); this response emulates potentiation in a biological synapse. Pre-synaptic APs at 50 Hz were applied alternately to two synaptic transistors that would be individually connected to a flexor and an extensor. The devices generated clear EPSC responses (Fig. 1e).

Each synaptic transistor was made of a single organic semiconducting nanowire, an ion-gel gate dielectric and inter-digitated source and drain electrodes on an elastomeric substrate (Supplementary Fig. 2a and Supplementary Note 1). The organic semiconducting nanowire, which emulates the shape of a neuron, was highly flexible and stretchable (100% strain) (Supplementary Figs. 2b and 3); it was fabricated by electrospinning and transferred onto a pre-strained elastomeric substrate[21,37]. A synaptic transistor array with a high resolution of 30 pixels per inch was also demonstrated by direct printing of highly aligned serpentine nanowire array on the substrate (Supplementary Fig. 4). The synaptic transistors maintained stable electrical characteristics under strain from 0% to 100% and after 1,000 times of repeated stretching to 100% strain in both parallel and perpendicular directions to the charge transport (nanowire) direction (Fig. 1f–i and Supplementary Fig. 5). This nanoscale channel dimension can enable low-energy operation[32,33].

When a pre-synaptic gate voltage V_G pulse is applied to the gate electrode, anions in the ion gel migrate and accumulate near the organic semiconducting nanowire (Supplementary Fig. 2c). Holes are temporarily induced to the nanowire from the source electrode, resulting in an EPSC. The devices showed uniform electrical characteristics (Supplementary Fig. 6). These post-synaptic signals are amplified, then applied to the muscles.

Muscle activation with SNEN

To quantify how the contraction of a muscle was affected by frequency f_{AP} of APs, we connected a single synaptic transistor to a knee flexor of an anaesthetized mouse's hind limb (Fig. 2a). Electromyography signals elicited electrophysiological activity of the muscle (Supplementary Fig. 7). As f_{AP} was increased from 1 Hz to 11 Hz, the maximum angular displacement increased from 6.67° to 40° (Fig. 2b–e and Supplementary Video 1). We measured the isometric force of the mouse's hind limb by stimulating an extensor AP with $1 \leq f_{AP} \leq 50$ Hz (Fig. 2f). The maximum force increased from 39 mN to 412 mN (4 g to 42 g) as f_{AP} increased (Fig. 2g). This change occurred because the muscle contraction response changed from weak contraction (twitch) at low f_{AP} to continuous and strong contraction (tetanus) at high f_{AP} (ref. [38]). The gradually increased muscle force response and smooth leg motion were achieved by a synaptic transistor in response to post-synaptic signal potentiation; this response is clearly different from the abrupt increase then decrease in muscle force, and drastic leg motion induced by conventional stimulation using electrical pulses of constant amplitude (Supplementary Fig. 8). To emulate synchronized movement, we connected two synaptic transistors, one to a flexor and one to an extensor (Fig. 2h). APs at $f_{AP} = 50$ Hz were applied alternately to the synaptic transistors at intervals of 1 s, and each muscle was stimulated to extend and flex in sequence (Fig. 2i–k, Supplementary Fig. 9 and Supplementary Video 2). Soft and stretchable electrically conductive hydrogel electrodes were used as the bio-interface to the muscles[39,40]. The nanoporous conductive polymer network gave high electrochemical surface area and low impedance of 0.5 kΩ at $f_{AP} = 1$ kHz. The hydrogel electrode (electrode area 8 mm^2) elicited higher angular displacement of the leg than did needle electrodes (25 G, electrode area 10 mm^2) (Fig. 2i,j).

Artificial proprioceptor and power-consumption analysis

Proprioception is required for basic motor functions such as standing and walking. The absence of proprioceptive feedback degrades the locomotion and damages muscles, and thereby impairs interactions between neuroprosthetics users and the physical environment. Therefore, restoring motor functions with proprioception in patients with neurological disorders has long been the goal in medicine and bioengineering[41]. However, development of methods to achieve proprioceptive feedback in neurorehabilitation devices is a challenge. An artificial muscle spindle-based proprioceptive feedback loop could provide unconditioned proprioceptive feedback to temporo-spatial coordination of limb movement, and prevent damage of muscle caused by overstraining.

We demonstrated an artificial proprioceptor to detect leg movement and prevent overstretching of the muscle (Fig. 3a,b). The artificial proprioceptor, together with the artificial synapse, formed a closed feedback loop (Fig. 3c). A sensor composed of CNTs was used to mimic the biological muscle spindle and to detect the extension of the leg. The sensitive CNT strain sensor was fabricated using a capillary-flow-based self-pinning effect. The sensor can operate with low hysteresis in the strain sensing range from 0% to 50%, similar to a previous report[42] with a resistance range from 100 kΩ to 3 MΩ (Fig. 3d,e).

We designed a negative feedback mechanism by mimicking the muscle spindle. EPSC can be downregulated by the leg extension and increase in resistance R_1 of the strain sensor (Fig. 3b). With a large strain, the voltage divider circuit lowers the effective gating voltage to the synaptic transistor by increasing R_1 ($V_2 = 0$ V) (Fig. 3f and Supplementary Fig. 10). The proprioceptive sensitivity was controlled using $V_2 > 0$ V. This negative feedback gradually limited potentiation of the EPSCs of synaptic transistors to asymptotes according to the applied V_2; the maximum EPSC of 1.03 μA ($V_2 = 0$ V, with low-sensitivity feedback) was limited to 0.73 μA ($V_2 = 1.5$ V, with high-sensitivity feedback) (Fig. 3g,h,

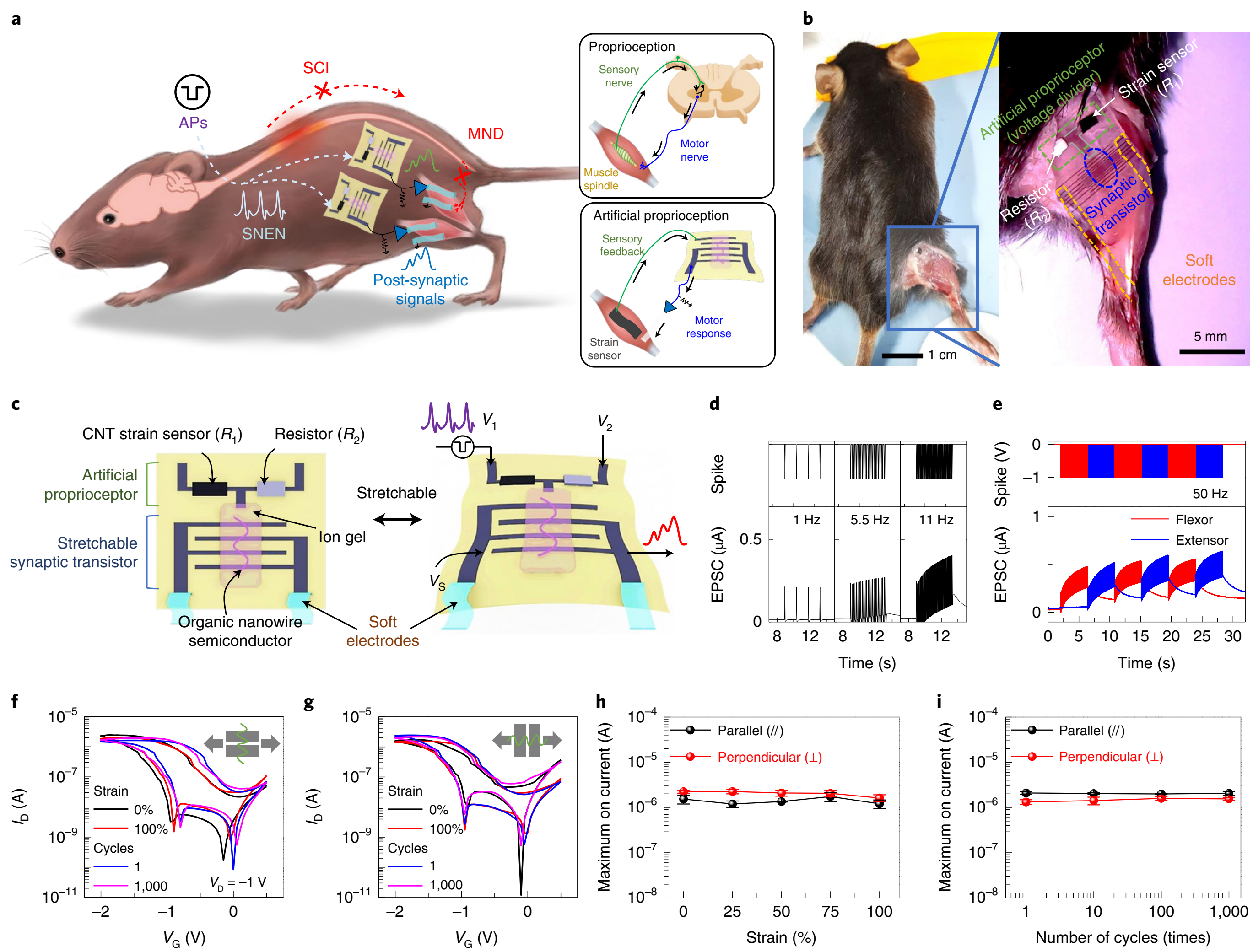

Fig. 1 | SNEN. a, Schematics of SNEN based on organic electronic synapses that bypass the damaged nerves and relay neural signals to the muscle. **b**, Photographs of anaesthetized mouse with SNEN attached to the leg. Flexors and extensors of the legs are electrically stimulated by post-synaptic signals through soft electrodes or needle electrodes. **c**, Stretchable components of SNEN composed of an artificial proprioceptor with a CNT strain sensor, a stretchable synaptic transistor with organic semiconducting nanowire, inter-digitated CNT electrodes, and ion-gel dielectric on elastomer substrate, and soft hydrogel electrodes. **d**, Pre-synaptic voltage spikes that are applied to the gate electrode and EPSCs that are read by the drain electrodes with spike firing frequencies of 1, 5.5 and 11 Hz. **e**, EPSCs from two synaptic transistors that are individually connected to a flexor (red) and an extensor (blue) with spike firing frequency of 50 Hz. **f**,**g**, *I*–*V* characteristics of synaptic transistor at 0% and 100% strains, and after 1,000 times of repeated stretching at 100% strain in parallel (//) (**f**) and perpendicular (⊥) (**g**) directions to the nanowire channel. **h**,**i**, Maximum on current as a function of various strains (**h**) and after stretching cycles at 100% strain (**i**) in parallel (//) and perpendicular (⊥) directions to the nanowire channel ($n=3$). Error bars denote standard deviation (s.d.).

Supplementary Note 2, Supplementary Table 1 and Supplementary Figs. 11 and 12). The artificial efferent nerve should have simultaneous excitatory and inhibitory synaptic responses to prevent overstretching of muscle, similar to the biological stretch reflex. Therefore, the proprioceptive feedback is necessary to effectively limit excitatory synaptic response and resultant muscle contraction in real time. In the presence of feedback, the leg flexion motion was stable, but in the absence of feedback, it was shaky owing to over-strain (Supplementary Fig. 13). Our approach also enabled artificial proprioception during repeated motions to prevent muscle damage caused by overstraining (Supplementary Fig. 14).

The increase of resistance of the strain sensor leads to reduced current flow and consequently a decrease in power consumption in the 'on' state. In detail, the SNEN consumes ~4.55 μW ('on' state) and ~5.33 μW ('off' state) (Supplementary Note 3, Supplementary Tables 2–5 and Supplementary Fig. 15). Also, with I/V converter, the power consumption of SNEN system is 23.8 μW ('on' state) and 7.96 μW ('off' state) (Supplementary Note 3, Supplementary Fig. 16 and Supplementary Table 5).

Simulation of power calculation of an array of the SNEN system suggests that its power consumption (6.1 mW) is two orders of magnitude lower than a system composed of a one-transistor/one-strain sensor array connected to silicon integrated circuit chips with a microprocessor (928 mW) (Supplementary Figs. 17 and 18 and Supplementary Table 6). The reduction occurs because the SNEN system operates only in response to events[31,33] whereas the silicon integrated circuit chips with a microprocessor operate continuously.

The organic components are stable for long-term usage. A long-term stability test of a CNT strain sensor and a soft hydrogel electrode encapsulated by styrene-ethylene-butylene-styrene (SEBS) was conducted in phosphate-buffered saline (PBS; 1X, pH 7.4) solution with accelerated ageing time at 60 °C (refs. [43,44]) (Supplementary Note 4).

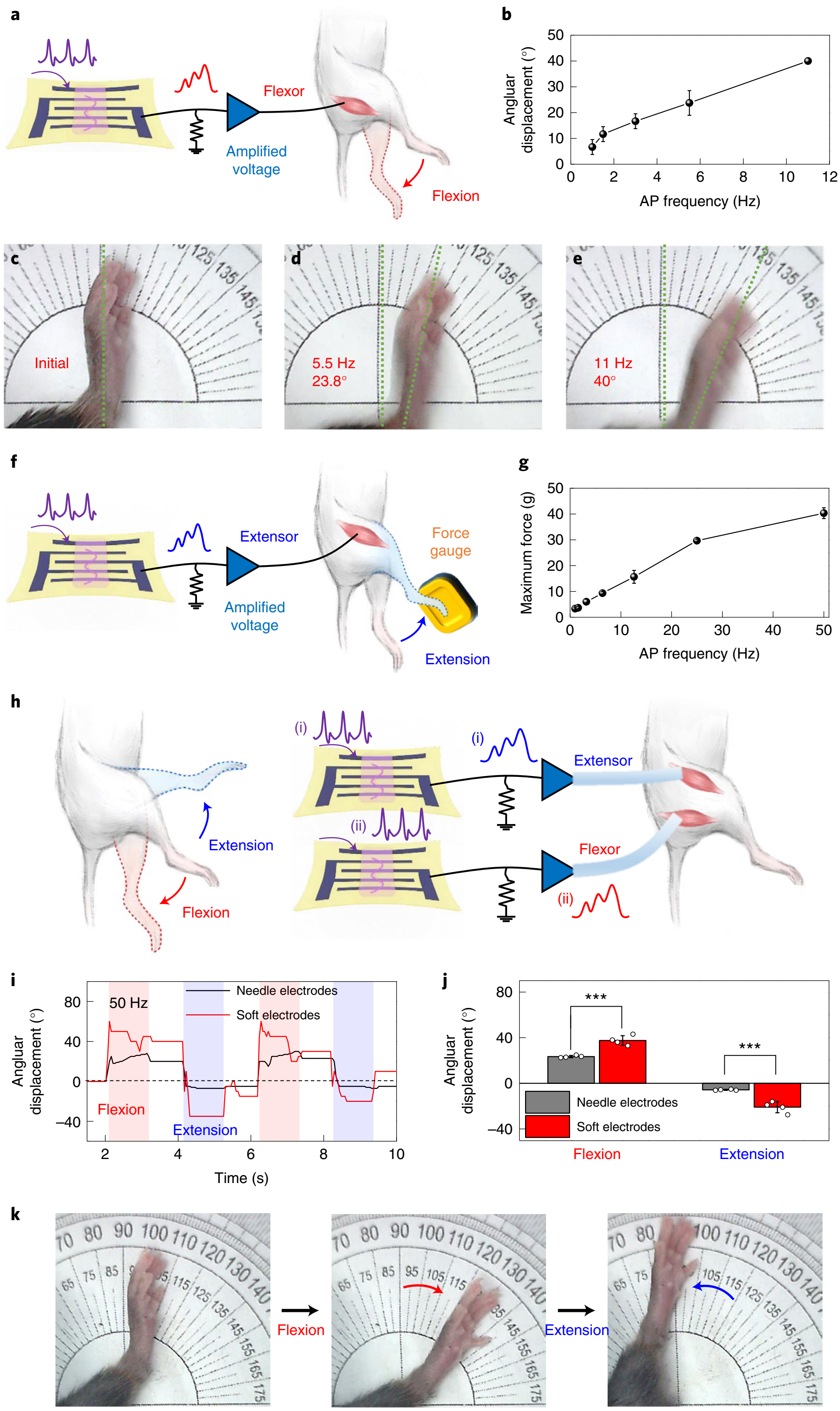

Fig. 2 | Muscle contraction. a, Stimulation of a flexor of a hind leg with an artificial efferent nerve. **b**, Angular displacement of a hind leg depending on f_{AP} from 1 Hz to 11 Hz ($n=4$). **c**–**e**, Photographs of the leg motion at f_{AP} of 0 (**c**), 5.5 (**d**) and 11 Hz (**e**). **f**, Stimulation of an extensor of a hind leg with an artificial efferent nerve. **g**, Maximum force of a hind leg depending on f_{AP} from 1 Hz to 50 Hz ($n=4$). **h**, Stimulation of an extensor and flexor of a hind leg with two artificial efferent nerves; one nerve was connected to an extensor and the other nerve was connected to a flexor. **i**,**j**, Angular displacement (**i**) and uniformity (**j**) of a hind leg depending on the alternate stimulation of the flexor (flexion) and extensor (extension) with needle electrodes (25 G) and soft electrodes (electrode size 8 mm^2). The P values for comparison of the needle and soft electrodes are 0.0006 for flexion and 0.0008 for extension. $^{***}P<0.001$. Unpaired, two-tailed t-test ($n=4$). **k**, Photographs of leg motion with flexion and extension. All error bars denote s.d.

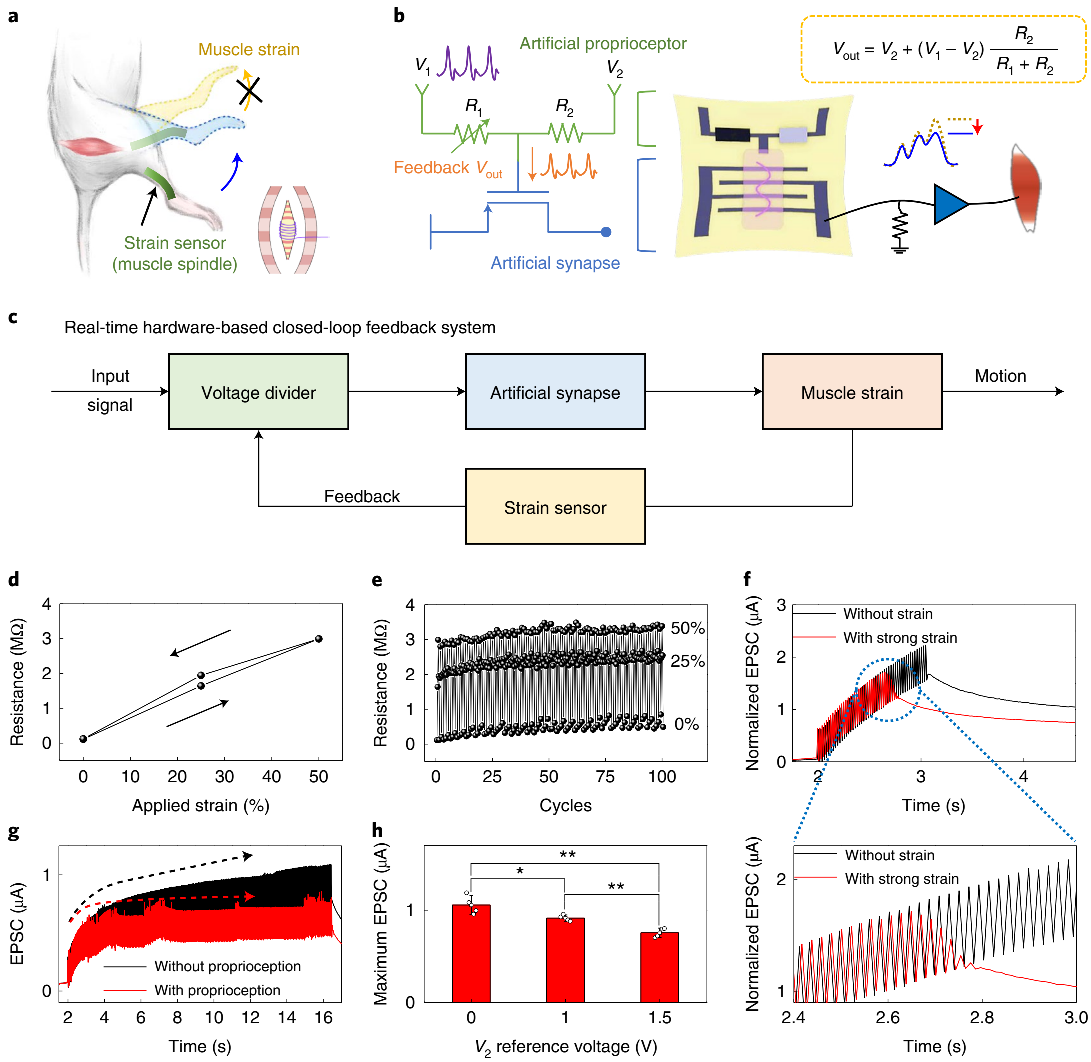

Fig. 3 | Artificial proprioception. a,**b**, Conceptual design (**a**) and schematic (**b**) of an artificial muscle spindle-based proprioceptive feedback loop that prevents damage of muscle caused by overstraining. **c**, Block diagram of the real-time hardware closed-loop feedback system of artificial proprioception. **d**,**e**, Resistance change of the CNT strain sensor (artificial muscle spindle) with low hysteresis (**d**) and cyclic stability (**e**). **f**, Normalized EPSCs (I–$I_{Baseline}$) without strain (black) and with strong strain (red). **g**, EPSCs without proprioceptive feedback (black) and with proprioceptive feedback (red). **h**, Maximum EPSCs modulated by proprioceptive feedback according to the reference voltage V_2. The P values for comparison of the reference voltage are as follows: for V_2 = 0 V versus 1 V, P = 0.04; for V_2 = 1 V versus 1.5 V, P = 0.002; and for V_2 = 0 V versus 1.5 V, P = 0.0019. *$P \leq 0.05$ and **$P \leq 0.01$. Unpaired, two-tailed t-test (n = 4). Error bars denote s.d.

With ageing factor Q_{10} = 2, the resistance of the strain sensor and the soft electrode was stable for 14 days at 60 °C, equivalent to 69 days at body temperature (T_{BT}, 37 °C) (Supplementary Fig. 19a,b). A stability test of a synaptic transistor (Supplementary Fig. 20 and Supplementary Note 4) encapsulated by polydimethylsiloxane (ref. [36]) was conducted in PBS solution with accelerated ageing time at 60 °C. The maximum on current and threshold voltage V_{th} of the synaptic transistor was maintained stably for 6 days at 60 °C (Supplementary Fig. 19c–e); with ageing factor Q_{10} = 2; this is equivalent to 30 days at T_{BT}. The stability of synaptic transistor was also measured in air ambient condition during 14 days and showed uniform I–V characteristics. A device operated stably after being stored for ~2 years, but with slightly increased off-current, likely due to a moisture effect (Supplementary Fig. 19f,g).

Bipedal walking with SNEN

The feasibility of using the SNEN in practical locomotion was shown with a mouse suspended by a vertical supporter (Fig. 4a). Input signals were applied to the synaptic transistor that was connected to an extensor of the right hind leg (Extended Data Fig. 1a). The input signal patterns were regulated to control the swing motion of the leg. The EPSC signals were sufficient to elicit a sharp contraction of the extensor, so the leg could swing fully and kick a ball to a greater distance than hind leg length (Extended Data Fig. 1b,c and Supplementary Video 3).

We also implemented bipedal walking locomotion (Fig. 4b). One synaptic transistor was connected to the flexor in the left leg and the extensor in the right leg, while the other transistor was connected to the extensor in the left leg and the flexor in the right leg (Fig. 4c). Alternating input signals to each SNEN induced bipedal walking locomotion (Fig. 4d and Extended Data Fig. 2). By adjusting the input APs, we controlled the moving speed from slow walking (0.8 cm s^{-1}) to running (2.5 cm s^{-1}) on a treadmill (Fig. 4e–g and Supplementary Video 4). These results suggest that the SNEN has the potential to provide locomotion in living animals.

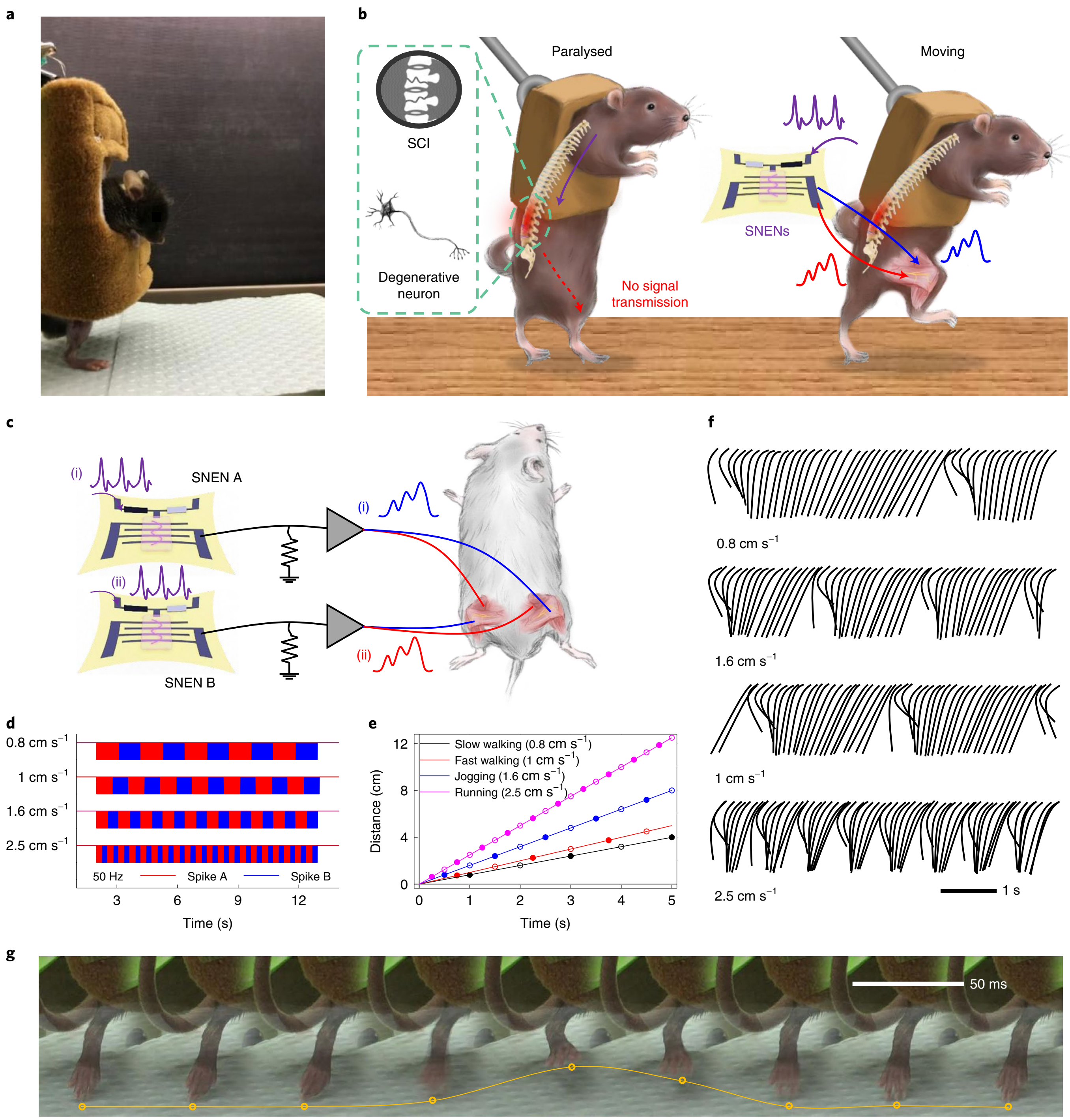

Fig. 4 | Bipedal walking locomotion. a,**b**, Photograph (**a**) and schematic (**b**) of a paralysed mouse afflicted by SCI or MND (left) and a mouse that had recovered voluntary motor function by using SNEN (right). Practical locomotion is demonstrated with coordinated stimulation of the muscles by post-synaptic signals of the SNEN and patterned pre-synaptic AP inputs. **c**, Configuration of the mouse for bipedal walking locomotion. **d**,**e**, Pre-synaptic input spike patterns (**d**) and moving distance (**e**) with different moving speeds (0.8 cm s^{-1}, slow walking; 1 cm s^{-1}, fast walking; 1.6 cm s^{-1}, jogging; 2.5 cm s^{-1}, running). **f**, Kinematic trajectory of a hind leg with different moving speeds. **g**, Photochronography of a hind leg during walking.

SNEN with electrophysiological signals

Furthermore, to demonstrate applicability of the SNEN in future neuromorphic neurorehabilitation devices, neural signals recorded from the animal's primary motor cortex during limb movement were used as pre-synaptic input signals for the artificial efferent nerve. Electrophysiological data of two single-unit recorded neurons was sampled from a public dataset[45] (Extended Data Fig. 3). The firing patterns of both neurons were used as the gate voltage of the synaptic transistor. Neuron 1 with a high firing rate (34.8 Hz) triggered a higher potentiated amplitude of EPSC than did neuron 2 that had a low firing rate (2.8 Hz) (Extended Data Fig. 3).

The device can process electrical inputs from multiple neurons. Electrophysiological data of seven single-unit recorded neurons (numbers 1–7) were extracted from the public dataset[45] (Fig. 5a,b).

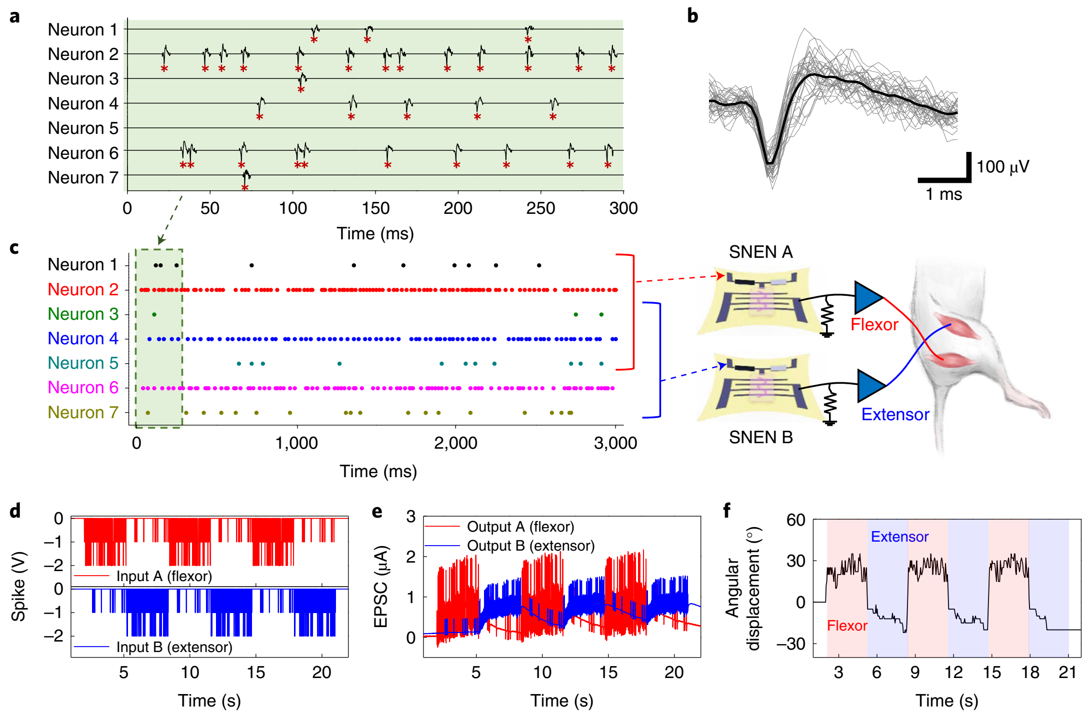

Fig. 5 | Electrophysiological signals. a–c, Illustration of electrophysiological data (**a**), waveforms (**b**), and neural spike raster plot (**c**) sampled from seven single-unit recorded neurons in the primary motor cortex of a moving animal from the CRCNS dataset[45]. Pre-synaptic input patterns composed of five neurons (numbers 1–5) projected to SNEN A, and five neurons (numbers 3–7) projected to SNEN B. SNENs A and B are interfaced with flexor and extensor, respectively, using needle electrodes. **d**,**e**, Pre-synaptic voltage spikes (**d**) and EPSCs (**e**) of synaptic transistors. **f**, Angular displacement of a hind leg depending on the alternate stimulation of the flexor (flexion) and extensor (extension).

Two pre-synaptic input signal patterns composed of combined signals from five neurons (numbers 1–5) were projected to SNEN A, and the combined signals from five neurons (numbers 3–7) were projected to SNEN B (Fig. 5c). SNEN A was interfaced with a flexor, and SNEN B was interfaced with an extensor (Fig. 5c). The device, as an analogue of an axon hillock, summed multiple neural inputs at different firing rates and yielded an output EPSC (Fig. 5d,e). Then the muscles were activated by the voltage signals converted from EPSC by I/V converter (Supplementary Note 5 and Supplementary Fig. 21). In the overall process, the SNEN received neural signals of motor cortex and initiated motion in the muscle, bypassing the spinal cord and peripheral nervous system. The two muscles were alternately stimulated, and executed different angular swing motions (Fig. 5f and Supplementary Fig. 22). The SNEN can relay single-unit electrophysiological signals to a muscle and cause muscle movement, and therefore has potential to take neural signals from the brain and control limb movement by using a simple device composed of one strain sensor and a synaptic transistor.

Discussion

We have reported an SNEN. The SNEN was operated with both simulated APs and extracellularly recorded public neural data as input, to stimulate muscles in the leg of an anaesthetized mouse, bypassing the spinal cord. The organic stretchable artificial synapses stably relay neural signals to the muscles. Similar to the biological voluntary motor response, the firing rate in the SNEN determines the motion and maximum force of the mouse's leg. We also demonstrate an artificial muscle spindle that detects the change of muscle length by using strain sensors, and enables a negative feedback loop. This proprioception function prevents muscle damage due to overstretching of the muscles. Furthermore, by implementing several locomotions such as 'kicking a ball' and 'walking/running' in living animals, the SNEN shows promise for the treatment of motor disorders caused by degenerative neural diseases.

This work shows that advanced functions of coordinated and complex leg motions can be elicited in living mammals via soft neural interfaces and stretchable electronic systems. This is a step towards a future artificial nerve system that could serve as a low-power neuromorphic prosthetic device that enables limb movement via motor-cortex-driven signals. In the future, simple systems such as the SNEN that use the principle of neuroplasticity may represent a promising bioengineering technology for the generation of voluntary motion in animals with motor disorders, obviating the need for heavy and complicated electronic devices.

Methods

Fabrication of electrospun organic nanowires[37]. Homogeneous mixture solution of fused thiophene diketopyrrolopyrrole (FT4-DPP)-based conjugated polymer poly[(3,7-bis(heptadecyl)thieno[3,2-*b*]thieno[2′,3′:4,5]thieno[2,3-*d*]thiophene-5,5′-diyl)(2,5-bis(8-octyloctadecyl)-3,6-di(thiophen-2-yl)pyrrolo[3,4-*c*]pyrrole-1,4(2H,5H)-dione-5,5′-diyl)] (provided by Corning Incorporated, number average molecular weight 33,000 g mol^{-1}, polydispersity index 2) and high-molecular-weight polyethylene oxide (Aldrich, weight average molecular weight 400,000 g mol^{-1}, 7:3 w:w) in chloroform was used to fabricate organic semiconducting nanowires by electrospinning (printing parameters: tip-to-substrate distance 15 cm, external voltage 3 kV, solution feeding rate 1 μl min^{-1}). Single nanowires were aligned between two parallel electrodes and transferred onto the substrate.

Fabrication of organic stretchable electronic synapse[21]. Inter-digitated CNT source–drain electrodes were fabricated by spray coating single-wall CNTs on hydrophobic SiO_2/Si substrate, then transferred onto free-standing SEBS substrate (500 μm). A single electrospun organic nanowire was located on a CNT-patterned SEBS substrate that had been pre-strained to 100%. When the strain was released, the highly flexible nanowire assumed a wavy structure that was stable after repeated mechanical deformation. Ion-gel gate dielectric of poly(styrene-*b*-methyl methacrylate-*b*-styrene) (PS-PMMA-PS) triblock co-polymer and 1-ethyl-3-methylimidazolium bis(trifluoromethylsulfonyl) imide ([EMIM][TFSI]) ionic liquid dissolved in ethyl acetate (0.7:9.3:90, w/w) was formed on the channel area by drop casting.

For the stability test in PBS solution, poly(vinylidene fluoride-hexafluoropropylene) was used as a matrix material of polymer gel electrolyte instead of PS-PMMA-PS triblock co-polymer and encapsulated by polydimethylsiloxane to enhance the device stability[36].

Fabrication of soft electrode[40]. Poly(3,4-ethylenedioxythiophene):poly(styrene sulfonate) (PEDOT:PSS) Orgacon ICP 1050 was provided by Agfa as a surfactant-free aqueous dispersion with 1.1 wt% solid content. Before use, the PEDOT:PSS dispersion was filtered through a 1.0-μm filter to remove any large agglomerates. Glycerol (G9012-100ML) was purchased from Sigma-Aldrich; 0.165 g of glycerol was added to 15 ml of PEDOT:PSS solution. The mixture was stirred vigorously at room temperature for 20 min. The PEDOT:PSS/glycerol aqueous mixture was then filtered through a 0.45-μm syringe filter. SEBS solution (0.1 g ml^{-1} in toluene) was drop cast on a glass slide and allowed to dry overnight. After the solvent had evaporated, the SEBS film was treated with oxygen plasma (Technics Micro-RIE Series 800, 150 W, 200 mTorr) for 1 min. The prepared PEDOT:PSS/glycerol aqueous mixture was spin coated on the SEBS film at 1,500 rpm, then annealed at 120 °C for 10 min. A polyethylene terephthalate mask (with 2 mm × 40 mm rectangular pattern cut using a Silhouette Cameo Cutter) was placed on the PEDOT:PSS/glycerol film, then dry-etched with oxygen plasma for 10 min. Another SEBS film was laminated on the PEDOT:PSS/glycerol/SEBS film to encapsulate the interconnect area. The soft electrode was annealed on a hotplate for 40 min at 120 °C. The electrode was soaked in 1X PBS for at least 2 h before in vivo application.

Fabrication of CNT strain sensor by using self-pinning effect[42]. A thin SEBS substrate (~100 μm) was prepared on the glass. The film mask with hollow patterns covered the surface of the SEBS. The uncovered surface was made hydrophilic by treating it with oxygen plasma (150 W, 20 s). The mask was detached, then a solution of single-wall CNTs was dropped on the hydrophilic patterns by using a micropipette, then dried at room temperature.

Device measurement. *Synaptic transistors.* Pre-synaptic voltage spikes were applied to the gate electrode ($V_G = -1$ V), and post-synaptic currents were read by the drain electrode ($V_D = -1$ V) with grounded source electrode.

SNEN. Pre-synaptic voltage spikes were applied to the gate electrode ($V_G = -1$ V) and a source voltage of 1 V. For muscle stimulation, the drain electrode was connected to I/V converter to amplify output signals.

In vivo experiment. *Preparation of mice.* Adult (25–35 g) male C57BL/6J mice (Jackson Laboratories) were group-housed, given access to food pellets and water ad libitum, and maintained on a 12 h:12 h light:dark cycle. All animals were held in a facility next to the laboratory starting 1 week before surgery, through post-surgery and throughout the duration of the behavioural assays to minimize stress due to transportation and disruption by foot traffic. All procedures were approved by the Animal Care and Use Committee of Stanford University (protocol APLAC-31893) and Institutional Animal Care and Committee of Seoul National University (protocol SNU-201105-3), and conform to US National Institutes of Health and Korea Food & Drug Administration guidelines.

For in vivo electrical stimulation on muscle, mice were acclimatized to the holding facility for more than 1 week, then anaesthetized using isoflurane or ketamine/xylazine or alfaxan/xylazine. A heating pad at 37 °C was placed underneath the body. To ensure that the animal was fully anaesthetized, we verified the absence of paw reflexes by pinching a hind paw with tweezers, and checked the absence of eye reflexes. We then shaved both legs from the knee to the hip by using an electrical shaver. Protective eye liquid gel was applied to the eyes with a cotton-tipped swab. We then disinfected the surgery field with chlorhexidine and 70% ethanol by wiping with a gauze pad or cotton-tipped swab. The depth of anaesthesia was monitored by pinching the feet of the mice periodically. A 2-cm incision was made in the skin to expose the rectus femoris and gastrocnemius muscles. Soft and elastic hydrogel electrodes (surface area 8 mm^2) or needle electrodes (25 G) were gently interfaced with the extensor and flexor muscles. After implantation, the skin was sutured using surgical knots. The electrodes were connected to the artificial proprioceptor and artificial synapses. Pre-synaptic gate voltage pulse was applied to the artificial synaptic transistor. The extracellular recording data were collected by Matthew G. Perich in the laboratory of Lee E. Miller at Northwestern University and downloaded from CRCNS.org[45]. Single-unit AP from the dataset was recorded from neurons in premotor cortex by using a multi-electrode array. The leg response was recorded using a digital microscope. The force generated by leg movement was measured by a force gauge placed next to the mouse leg.

Protractor marks printed on paper were placed under the leg to enable measurement of the swing angle. Electromyography was used to record muscle activity during electrical stimulation. Three needle electrodes were used to penetrate the muscles, and the electrodes were connected to a signal acquisition system (Muscle SpikerBox, Backyard Brain). To demonstrate the natural movement, such as kicking, walking and running, the mice were suspended with a vertical supporter on the ground. The mice were killed immediately after the experiment.

Reporting summary. Further information on research design is available in the Nature Research Reporting Summary linked to this article.

Data availability

The authors declare that all data supporting the findings of this study are available within the paper and its Supplementary Information. The raw and analysed datasets generated during the study are available from the corresponding authors on request.

Received: 2 June 2021; Accepted: 29 June 2022;
Published online: 15 August 2022

References

1. Feigin, V. L. et al. Global, regional, and national burden of neurological disorders, 1990–2016: a systematic analysis for the Global Burden of Disease Study 2016. *Lancet Neurol.* **18**, 459–480 (2019).
2. Eggers, R. et al. Timed GDNF gene therapy using an immune-evasive gene switch promotes long distance axon regeneration. *Brain* **142**, 295–311 (2019).
3. Hu, X. et al. Electric conductivity on aligned nanofibers facilitates the transdifferentiation of mesenchymal stem cells into schwann cells and regeneration of injured peripheral nerve. *Adv. Healthc. Mater.* **9**, 1901570 (2020).
4. Borton, D., Micera, S., Millan, J. D. R. & Courtine, G. Personalized neuroprosthetics. *Sci. Transl. Med.* **5**, 210rv2 (2013).
5. Capogrosso, M. et al. A brain–spine interface alleviating gait deficits after spinal cord injury in primates. *Nature* **539**, 284–288 (2016).
6. Ethier, C., Oby, E. R., Bauman, M. J. & Miller, L. E. Restoration of grasp following paralysis through brain-controlled stimulation of muscles. *Nature* **485**, 368–371 (2012).
7. Song, K.-I. et al. Adaptive self-healing electronic epineurium for chronic bidirectional neural interfaces. *Nat. Commun.* **11**, 4195 (2020).
8. Wang, J., Wang, H. & Lee, C. Mechanism and applications of electrical stimulation disturbance on motoneuron excitability studied using flexible intramuscular electrode. *Adv. Biosyst.* **3**, 1800281 (2019).
9. Broderick, B. J., O'Briain, D. E., Breen, P. P., Kearns, S. R. & ÓLaighin, G. A pilot evaluation of a neuromuscular electrical stimulation (NMES) based methodology for the prevention of venous stasis during bed rest. *Med. Eng. Phys.* **32**, 349–355 (2010).
10. Bijak, M. et al. Stimulation parameter optimization for FES supported standing up and walking in SCI patients. *Artif. Organs* **29**, 220–223 (2005).
11. Lee, Y. & Lee, T.-W. Organic synapses for neuromorphic electronics: from brain-inspired computing to sensorimotor nervetronics. *Acc. Chem. Res.* **52**, 964–974 (2019).
12. Park, H.-L. et al. Flexible neuromorphic electronics for computing, soft robotics, and neuroprosthetics. *Adv. Mater.* **32**, 1903558 (2020).
13. Lee, W. W. et al. A neuro-inspired artificial peripheral nervous system for scalable electronic skins. *Sci. Robot.* **4**, eaax2198 (2019).
14. Zhang, S. et al. Selective release of different neurotransmitters emulated by a p–i–n junction synaptic transistor for environment-responsive action control. *Adv. Mater.* **33**, 2007350 (2021).
15. Park, H. et al. Retina-inspired carbon nitride-based photonic synapses for selective detection of UV light. *Adv. Mater.* **32**, 1906899 (2020).
16. Wan, C. et al. An artificial sensory neuron with tactile perceptual learning. *Adv. Mater.* **30**, 1801291 (2018).
17. Qian, C. et al. Oxygen-detecting synaptic device for realization of artificial autonomic nervous system for maintaining oxygen homeostasis. *Adv. Mater.* **32**, 2002653 (2020).
18. Choi, Y., Oh, S., Qian, C., Park, J. H. & Cho, J. H. Vertical organic synapse expandable to 3D crossbar array. *Nat. Commun.* **11**, 4595 (2020).
19. Zhang, C. et al. Bioinspired artificial sensory nerve based on nafion memristor. *Adv. Funct. Mater.* **29**, 1808783 (2019).
20. Seo, D.-G. et al. Versatile neuromorphic electronics by modulating synaptic decay of single organic synaptic transistor: from artificial neural networks to neuro-prosthetics. *Nano Energy* **65**, 104035 (2019).
21. Lee, Y. et al. Stretchable organic optoelectronic sensorimotor synapse. *Sci. Adv.* **4**, eaat7387 (2018).
22. He, K. et al. An artificial somatic reflex arc. *Adv. Mater.* **32**, 1905399 (2020).
23. Wei, H. et al. Mimicking efferent nerves using a graphdiyne-based artificial synapse with multiple ion diffusion dynamics. *Nat. Commun.* **12**, 1068 (2021).
24. Shim, H. et al. Stretchable elastic synaptic transistors for neurologically integrated soft engineering systems. *Sci. Adv.* **5**, eaax4961 (2019).
25. Kim, S. et al. Artificial stimulus-response system capable of conscious response. *Sci. Adv.* **7**, eabe3996 (2021).

26. You, I. et al. Artificial multimodal receptors based on ion relaxation dynamics. *Science* **370**, 961–965 (2020).
27. Park, S. et al. Self-powered ultra-flexible electronics via nano-grating-patterned organic photovoltaics. *Nature* **561**, 516–521 (2018).
28. Tan, Y. J. et al. A transparent, self-healing and high-κ dielectric for low-field-emission stretchable optoelectronics. *Nat. Mater.* **19**, 182–188 (2020).
29. Li, P., Anwar Ali, H. P., Cheng, W., Yang, J. & Tee, B. C. K. Bioinspired prosthetic interfaces. *Adv. Mater. Technol.* **5**, 1900856 (2020).
30. Cai, P. et al. Biomechano-interactive materials and interfaces. *Adv. Mater.* **30**, 1800572 (2018).
31. Kim, Y. et al. A bioinspired flexible organic artificial afferent nerve. *Science* **360**, 998–1003 (2018).
32. Xu, W., Min, S.-Y., Hwang, H. & Lee, T.-W. Organic core–sheath nanowire artificial synapses with femtojoule energy consumption. *Sci. Adv.* **2**, e1501326 (2016).
33. Lee, Y., Park, H.-L., Kim, Y. & Lee, T.-W. Organic electronic synapses with low energy consumption. *Joule* **5**, 1–17 (2021).
34. You, I., Kong, M. & Jeong, U. Block copolymer elastomers for stretchable electronics. *Acc. Chem. Res.* **52**, 63–72 (2019).
35. Sekitani, T. et al. Ultraflexible organic amplifier with biocompatible gel electrodes. *Nat. Commun.* **7**, 11425 (2016).
36. Sim, K. et al. An epicardial bioelectronic patch made from soft rubbery materials and capable of spatiotemporal mapping of electrophysiological activity. *Nat. Electron.* **3**, 775–784 (2020).
37. Lee, Y. et al. Deformable organic nanowire field-effect transistors. *Adv. Mater.* **30**, 1704401 (2018).
38. Head, S. I. & Arber, M. B. An active learning mammalian skeletal muscle lab demonstrating contractile and kinetic properties of fast- and slow-twitch muscle. *Adv. Physiol. Educ.* **37**, 405–414 (2013).
39. Liu, Y. et al. Soft and elastic hydrogel-based microelectronics for localized low-voltage neuromodulation. *Nat. Biomed. Eng.* **3**, 58–68 (2019).
40. Liu, Y. et al. Morphing electronics enable neuromodulation in growing tissue. *Nat. Biotechnol.* **38**, 1031–1036 (2020).
41. Formento, E. et al. Electrical spinal cord stimulation must preserve proprioception to enable locomotion in humans with spinal cord injury. *Nat. Neurosci.* **21**, 1728–1741 (2018).
42. Liu, Z. et al. Thickness-gradient films for high gauge factor stretchable strain sensors. *Adv. Mater.* **27**, 6230–6237 (2015).
43. Minnikanti, S. et al. Lifetime assessment of atomic-layer-deposited Al_2O_3–parylene C bilayer coating for neural interfaces using accelerated age testing and electrochemical characterization. *Acta Biomater.* **10**, 960–967 (2014).
44. Hukins, D. W. L., Mahomed, A. & Kukureka, S. N. Accelerated aging for testing polymeric biomaterials and medical devices. *Med. Eng. Phys.* **30**, 1270–1274 (2008).
45. Perich, M. G. et al. *Extracellular Neural Recordings from Macaque Primary and Dorsal Premotor Motor Cortex during a Sequential Reaching Task.* (CRCNS, 2018); https://doi.org/10.6080/K0FT8J72

Acknowledgements

This work was supported by the Creative-Pioneering Researchers Program through Seoul National University (SNU), the National Research Foundation of Korea (NRF) grant funded by the Korean government (Ministry of Science and ICT) (grant no. NRF-2016R1A3B1908431), and the Pioneer Research Center Program through the National Research Foundation of Korea funded by the Ministry of Science, ICT & Future Planning (grant no. NRF-2022M3C1A3090825). Y. Liu acknowledges National Science Scholarship (NSS) funding support from Agency for Science Technology and Research Singapore (A*STAR).

Author contributions

Y. Lee, Y. Liu, D.-G.S., Z.B. and T.-W.L. conceived of and designed the overall experiments. Y. Lee, Y. Liu and D.-G.S. conducted experiments and collected related data. J.Y.O. helped to fabricate synaptic transistors. Y.K. contributed to analysis of electrical circuit. J.L. helped with experiments on mice. J. Kang, J. Kim and J.M. contributed to strain sensor fabrication and measurements. A.M.F. aided in image visualization. Y. Lee, Y. Liu, D.-G.S., Z.B. and T.-W.L. analysed all data and co-wrote the paper. All authors discussed the results and commented on the manuscript.

Competing interests

The authors declare no competing interests.

Additional information

Extended data is available for this paper at https://doi.org/10.1038/s41551-022-00918-x.

Supplementary information The online version contains supplementary material available at https://doi.org/10.1038/s41551-022-00918-x.

Correspondence and requests for materials should be addressed to Zhenan Bao or Tae-Woo Lee.

Peer review information *Nature Biomedical Engineering* thanks Silvestro Micera, Cunjiang Yu and the other, anonymous, reviewer(s) for their contribution to the peer review of this work.

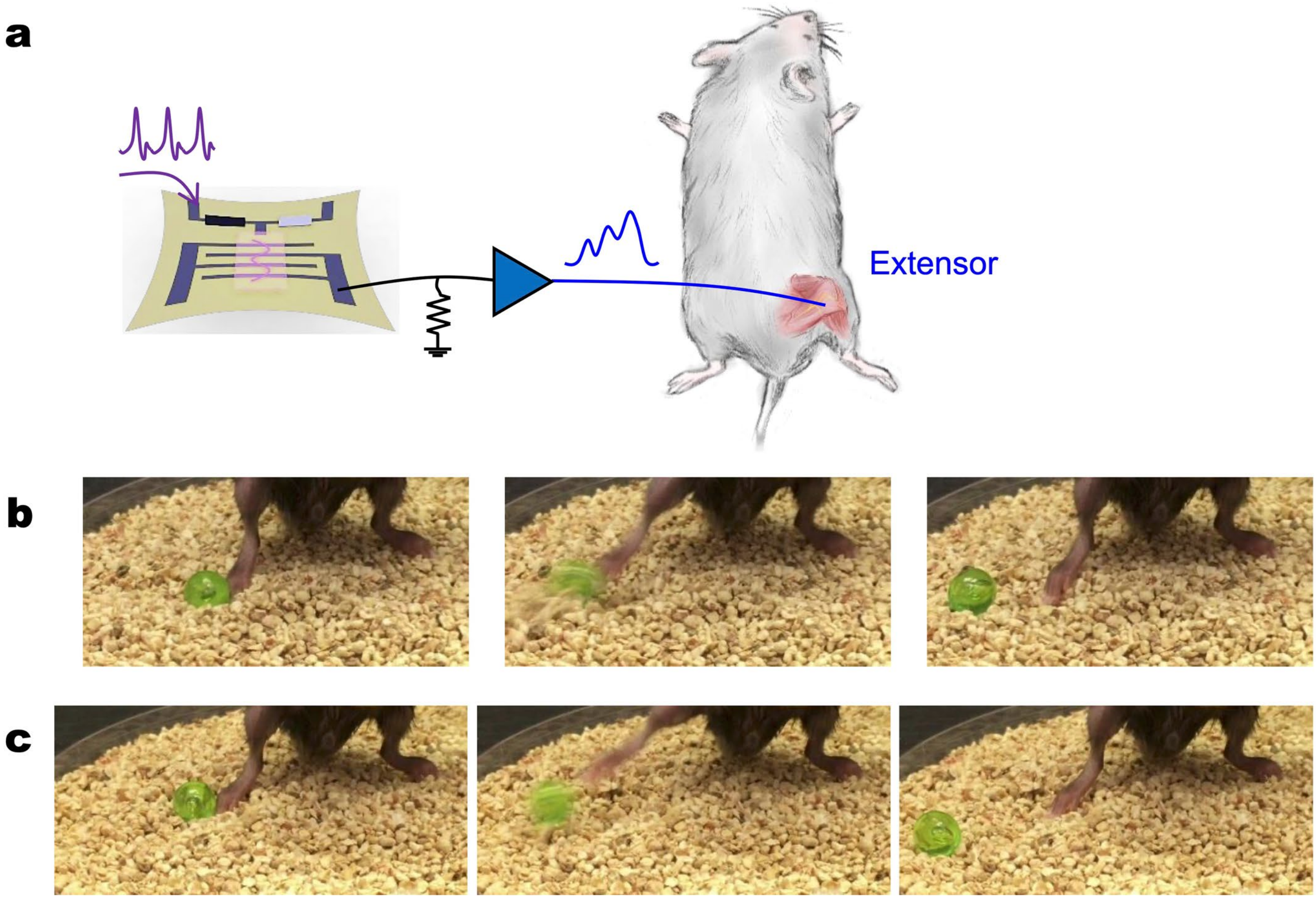

Extended Data Fig. 1 | Demonstration of practical locomotion of 'kicking a ball'. a, Design of the mouse for kicking a ball. An extensor was connected to SNEN system and the swing motion was controlled by synaptic signals. **b**,**c**, Photographs of the mouse kicking a ball with a weak and short muscle contraction (a small swing) (**b**) and a strong and long muscle contraction (a full swing) (**c**).

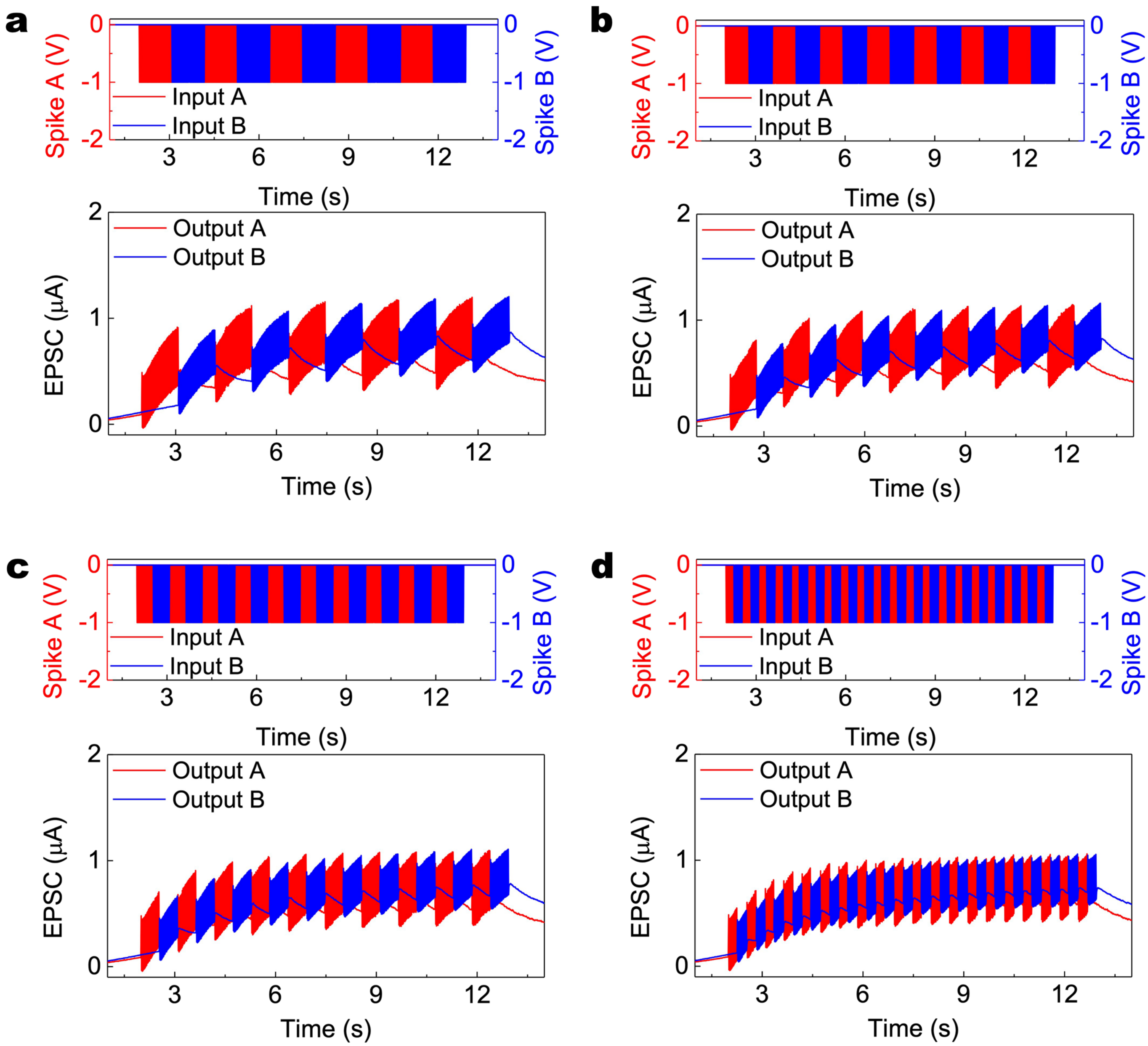

Extended Data Fig. 2 | Signals of SNEN for bipedal walking locomotion. a–d, Presynaptic input spike patterns (upper) and resultant EPSCs (lower) with different moving speeds of 0.8 cm/s (slow walking) (**a**), 1 cm/s (fast walking) (**b**), 1.6 cm/s (jogging) (**c**), and 2.5 cm/s (running) (**d**).

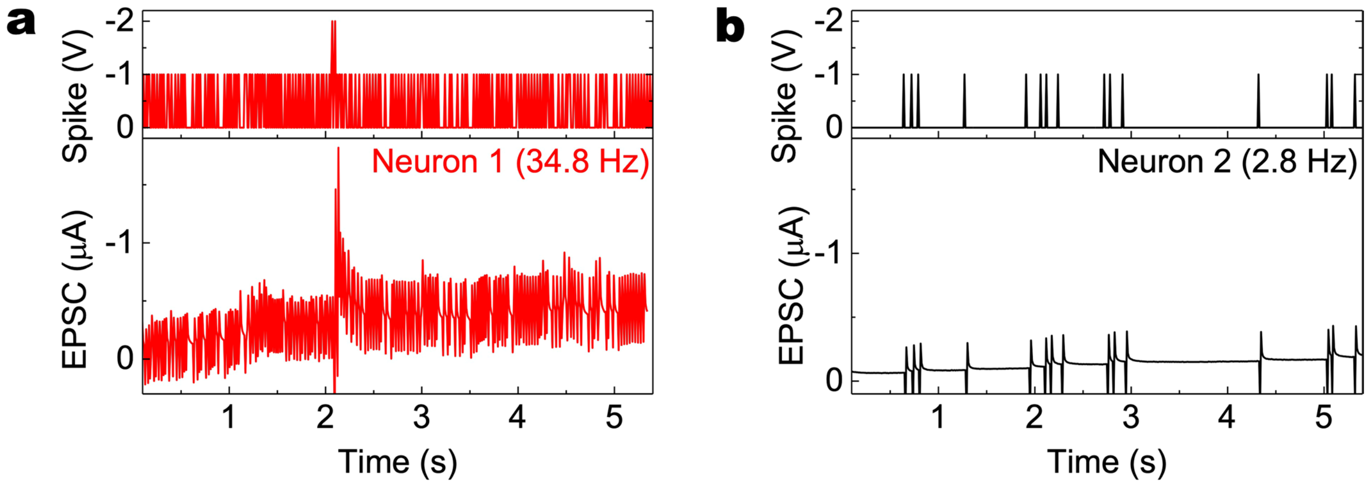

Extended Data Fig. 3 | SNEN with electrophysiological signals with different firing rates. a, **b**, Presynaptic input spike patterns referred from neural data (**a**) and resultant EPSCs (**b**) with high firing rate (34.8 Hz) (neuron 1, red) and low firing rate (2.8 Hz) (neuron 2, black).

nature portfolio

Corresponding author(s): Zhenan Bao, Tae-Woo Lee

Last updated by author(s): Mar 13, 2022

Reporting Summary

Nature Portfolio wishes to improve the reproducibility of the work that we publish. This form provides structure for consistency and transparency in reporting. For further information on Nature Portfolio policies, see our Editorial Policies and the Editorial Policy Checklist.

Statistics

For all statistical analyses, confirm that the following items are present in the figure legend, table legend, main text, or Methods section.

n/a	Confirmed	
☐	☒	The exact sample size (*n*) for each experimental group/condition, given as a discrete number and unit of measurement
☐	☒	A statement on whether measurements were taken from distinct samples or whether the same sample was measured repeatedly
☐	☒	The statistical test(s) used AND whether they are one- or two-sided *Only common tests should be described solely by name; describe more complex techniques in the Methods section.*
☒	☐	A description of all covariates tested
☒	☐	A description of any assumptions or corrections, such as tests of normality and adjustment for multiple comparisons
☐	☒	A full description of the statistical parameters including central tendency (e.g. means) or other basic estimates (e.g. regression coefficient) AND variation (e.g. standard deviation) or associated estimates of uncertainty (e.g. confidence intervals)
☐	☒	For null hypothesis testing, the test statistic (e.g. *F*, *t*, *r*) with confidence intervals, effect sizes, degrees of freedom and *P* value noted *Give P values as exact values whenever suitable.*
☒	☐	For Bayesian analysis, information on the choice of priors and Markov chain Monte Carlo settings
☒	☐	For hierarchical and complex designs, identification of the appropriate level for tests and full reporting of outcomes
☒	☐	Estimates of effect sizes (e.g. Cohen's *d*, Pearson's *r*), indicating how they were calculated

Our web collection on statistics for biologists contains articles on many of the points above.

Software and code

Policy information about availability of computer code

Data collection	The electronic-performance data of the synaptic transistor and stretchable artificial nerve were collected by means of the Model 4200-SCS Keithley Test EnvironmentInteractive (KTEI, Tektronix).
Data analysis	Data were analysed via OriginPro 2016 b9.3.226 (64-bit), Matlab R2017a and Microsoft Excel 2016 (version 1807,10325.20082). P-values were calculated via Prism.

For manuscripts utilizing custom algorithms or software that are central to the research but not yet described in published literature, software must be made available to editors and reviewers. We strongly encourage code deposition in a community repository (e.g. GitHub). See the Nature Portfolio guidelines for submitting code & software for further information.

Data

Policy information about availability of data

All manuscripts must include a data availability statement. This statement should provide the following information, where applicable:

- Accession codes, unique identifiers, or web links for publicly available datasets
- A description of any restrictions on data availability
- For clinical datasets or third party data, please ensure that the statement adheres to our policy

The authors declare that all data supporting the findings of this study are available within the paper and its Supplementary Information. The raw and analysed datasets generated during the study are available from the corresponding authors on request.

Field-specific reporting

Please select the one below that is the best fit for your research. If you are not sure, read the appropriate sections before making your selection.

☒ Life sciences ☐ Behavioural & social sciences ☐ Ecological, evolutionary & environmental sciences

For a reference copy of the document with all sections, see nature.com/documents/nr-reporting-summary-flat.pdf

Life sciences study design

All studies must disclose on these points even when the disclosure is negative.

Sample size	Sample sizes were not calculated beforehand. The sample size was determined by the number of biological and technical replicates necessary to convince us that the effect was real. We aimed for at least three biological replicates, and obtained several technical replicates for each sample.
Data exclusions	No data were excluded from the analyses.
Replication	All experimental findings were reliably reproduced.
Randomization	The experimental groups were formed based on what was being tested, with random selections.
Blinding	Blinding was not relevant to this study.

Reporting for specific materials, systems and methods

We require information from authors about some types of materials, experimental systems and methods used in many studies. Here, indicate whether each material, system or method listed is relevant to your study. If you are not sure if a list item applies to your research, read the appropriate section before selecting a response.

Materials & experimental systems

n/a	Involved in the study	
☒	☐	Antibodies
☒	☐	Eukaryotic cell lines
☒	☐	Palaeontology and archaeology
☐	☒	Animals and other organisms
☒	☐	Human research participants
☒	☐	Clinical data
☒	☐	Dual use research of concern

Methods

n/a	Involved in the study	
☒	☐	ChIP-seq
☒	☐	Flow cytometry
☒	☐	MRI-based neuroimaging

Animals and other organisms

Policy information about studies involving animals; ARRIVE guidelines recommended for reporting animal research

Laboratory animals	Adult (25–35 g) male C57BL/6J mice (Jackson Laboratories) were used.
Wild animals	The study did not involve wild animals.
Field-collected samples	The study did not involve samples collected from the field.
Ethics oversight	All procedures involving implantation and electrical stimulation were performed in accordance with protocols approved by the Institutional Animal Care and Use Committee (IACUC) at Stanford University and Seoul National University.

Note that full information on the approval of the study protocol must also be provided in the manuscript.